Supplementary Materials: Poms et al.

Sequences:

The following figure depicts a snake-plot of the Ste2p receptor, indicating the domain borders of the different proteins described in this study.
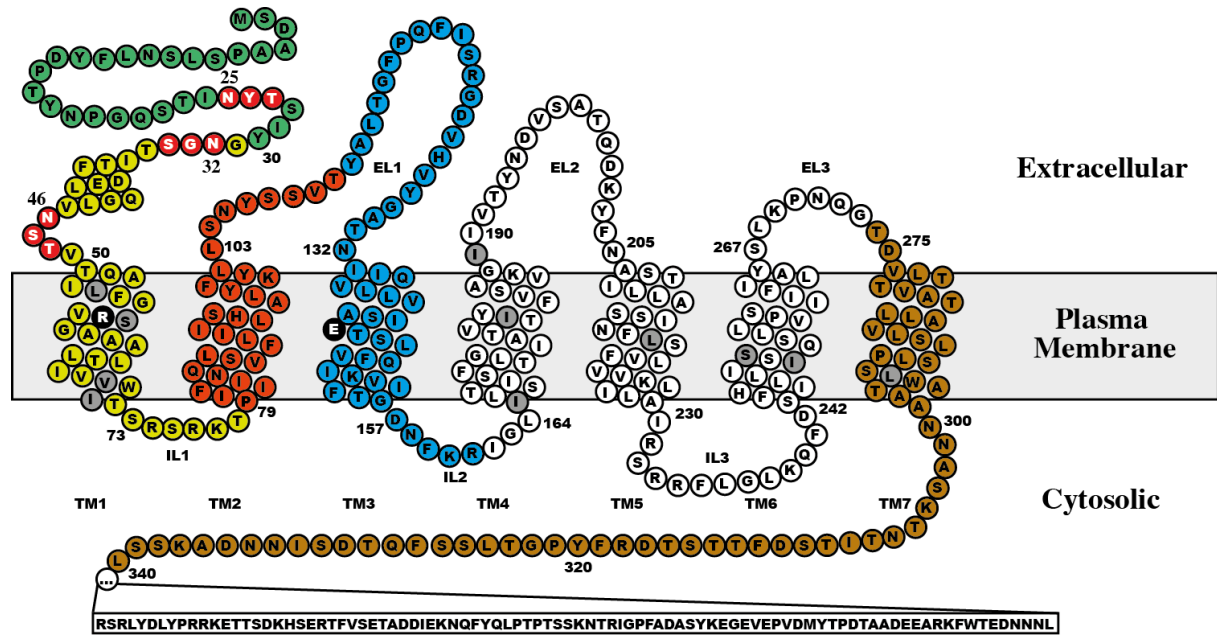

Figure S1: **Snake plot of the Ste2p receptor**. Positions originally occupied by Cys residues are highlighted in green. The charged residue Arg58 and Glu143 are depicted in black. Potential glycosylation acceptor sites NXS/T are highlighted in red. Constructs containing the full N-terminus as well as truncated forms starting at Gly30 have been used (see text). Note that in TM127 part of the EL1 as well as EL3 were used.

Cloning procedures:

Construction of the Ste2p TM127 (*G31-T114, T274-L340*) expression vector was accomplished using a two-step process. PCR was performed using primers designed to remove residues G115-G273 and the pBluescriptSK(-) BEC2(M54L, M69V, M71I, M165I)

Ste2p vector as a template. The resulting sequence was PCR amplified using a forward primer containing a *Hind*III site and a sequence complementary to the N-terminal sequence of the TM127 construct, and a reverse primer containing a *Bam*HI site and a sequence complementary to the C-terminal sequence of the TM127 construct. The amplified fragment and the pSW02 vector were digested with *Hind*III and *Bam*HI, gel purified, ligated using T4 DNA ligase, and transformed into DH5α. DNA from some of the resulting colonies was purified and sequenced. The resulting plasmid, pSW127, contained the TrpΔLE leader sequence in phase with Ste2p(G31-T114,T274-L340, M54L, C59S, M69V, M71I, M294L).

Cyanogen bromide cleavage did not result in pure proteins in case of the Cys mutants required for the PRE studies. Therefore, three different expression vectors were constructed for direct expression of TM127. One contained the full native N-terminus of Ste2p (S2-T114, T274-L340), and two additional constructs containing either a N- or C-terminal His_{10}-tag. The N-TM127 fragment was derived from the expression vectors pSW127 and pRE01. The latter plasmid contains the N-terminus in front of the TM1-TM3 fragment. Both plasmids were used as templates to construct N-TM1-TM2-TM7 using suitable overlapping primers in the TM1 region, a forward primer containing a *Nde*I restriction site and a reverse primer containing a *Bam*HI site. The amplified fragments, as well as the pSW02 vectors, were digested with *Nde*I and *Bam*HI, gel purified, ligated using T4 DNA ligase, and transformed into DH5α cells. Several colonies were picked and sequenced, resulting in the verified pMP01 expression vector containing N-TM127. N- and C-terminal His_{10}-tags were introduced using FX cloning (1). The only construct with high levels of expression was the one containing the N-terminal His-tag and a full N-terminus. The construct also contained a C3 cleavage site (Leu-Glu-Val-Leu-Phe-Gln-Gly-Pro) between the His-tag and Ser2. As the addition of the full terminus already added 30 residues to the original construct, we refrained from performing the C3 cleavage. The N-TM127 insert was amplified using the pMP01 vector as template with primers encompassing *Sap*I restriction sites. Precompiled FX cloning vectors were used, containing ORF-verified sequences of either N- or C-terminal His_{10}-tags with a C3 protease cleavage site adjacent to the HIS_{10}-tag. The insert and vectors were mixed, digested using *Sap*I, ligated using T4 DNA ligase, transformed into DH5α cells and sequenced, resulting in expression vectors pMP02 (His-N-TM127) and pMP03 (N-TM127-His). Point mutations of single Cys residues were introduced using standard Quickchange® protocols. Using the vector containing the HIS-N-TM127 insert as a template, three cysteine mutants were designed, His_{10}-N-TM127(S47C), His_{10}-N-TM127(S75C) and His_{10}-N-TM127(S104C).

The Ste2p TM1(G31-T78) construct was cloned as a direct expression vector from a vector encoding TM1-TM3, that itself was constructed from the vector pKC01, that contains the ΔTrp fusion of TM1-TM3. The TM1-TM3 direct expression vector, pRE01, was constructed by PCR amplification of the G31-R161 region of the Ste2p sequence from the pKC01 vector using a forward primer containing a His tag and an *Nde*I restriction site and a TM3 reverse primer containing a *Bam*HI restriction site. The resulting PCR product and the pKC01 vector were digested with *Nde*I and *Bam*HI. The digests were gel purified and then ligated using T4 DNA ligase. The resulting reaction mixture was transformed into DH5α and the DNA was purified and sequenced. The amplified plasmid, pRE01, contained a 6 residue His tag in frame with Ste2p(G31–R161, M54L, C59S, M69V, M71I).

Double stranded mutagenesis was performed on this pRE01 plasmid using primers designed to incorporate two stop codons after residue T78. The resulting PCR product was digested with *Dpn*I. The digested DNA was transformed into DH5α, ten colonies were isolated, and the plasmid DNA was extracted from each of the colonies. The extracted DNA was sent for sequencing. The resulting expression vector, pKC03, contained a 6 residue His tag in frame with Ste2p(G31-T78, M54L, C59S, M69V, M71I).

Truncates of Ste2p for the glycosylation assays were prepared by PCR amplification of the appropriated fragment. The 3' end primers, added the sequence GSMGSMGSM**NST**MMS (with a glycosylation acceptor site shown in bold) or alternatively GSMGSMGSM**Q**STMMS (with a mock glycosylation tag, non-acceptor Gln shown in bold), followed by tandem translation stop codons, TAG and TAA. The TM1 region from Ste2p was PCR amplified and cloned into the modified Lep sequence from pGEM plasmid between *Spe*I and *Kpn*I sites (2). The mutations Arg58Leu, Arg58Ala, Arg58Glu and Ser59Leu were performed with the QuikChange mutagenesis kit from Stratagene (La Jolla, CA), according to the manufacturer's protocol.

Expression of selectively reverse methyl labeled constructs:

ΔTrp-TM1-TM3 was also expressed to selectively protonate the methyl carbons of the isoleucine, leucine and valine (I, L, V, respectively) in an otherwise perdeuterated background[41]. This was accomplished using 2-keto-3-methyl-d,3-d$_1$-1,2,3,4-^{13}C butyrate and 2-keto-3-d$_2$-1,2,3,4-^{13}C butyrate as the metabolic precursors for V and L and I, respectively. The pKC01 expression vector was transformed into BL-21 AI cells. A small pre-culture was prepared in LB and used to inoculate 100 mL of M9 minimal medium prepared with ^{15}NH$_4$Cl,

[^{13}C]-glucose, and D_2O. The 100 mL culture was grown to OD_{600} of 0.4 and then diluted to 200 mL with M9 minimal medium prepared with $^{15}NH_4Cl$, ^{13}C-glucose, and D_2O. The 200 mL culture was grown to OD_{600} of 0.4 and then diluted to 1L with M9 minimal medium prepared with $^{15}NH_4Cl$, [^{13}C]-glucose, D_2O, and the labeled I, L, V metabolic precursors. The cells were again grown to OD_{600} of 0.4, expression was induced with 0.2% L-arabinose, and the culture was incubated at 37°C for 9.5 h. After the incubation, the cells were pelleted by centrifugation, and IBs were prepared as previously described [3].

For selective reverse methyl labeling of TM127, the pSW127 plasmid was transformed into BL21 Star(DE3)pLysS cells. 1 mL of LB (H_2O)/Cam,Amp overnight culture was used to inoculate 6 mL of LB (D_2O)/Cam, Amp culture and grown overnight. 1.5 mL of this overnight culture was subsequently transferred to 40 mL M9 (D_2O)/50% Cam, 20% Amp medium with $^{15}NH_4Cl$ as well as [^{13}C]-glucose, grown to OD_{600} of 1.2 and added to 1L of M9 medium. After growth to an OD_{600} of 1.0, the culture was cooled to 22ºC, metabolic precursors were added, and expression was induced with 0.5 mM IPTG for 18 h. Subsequently, the cells were harvested, lysed by ultra-sonication for 10 minutes, inclusion bodies were isolated by centrifugation at 14000 rpm for thirty minutes and aliquoted into 8 equal parts to not overload the column.

Fragment Stability:

Sample stability was analyzed by applying 50μl of freshly prepared NMR sample on a Superdex 200 10/300 GL size exclusion chromatography column in 40mM K_3PO_4 buffer (pH 6.4) containing 12mM LPPG, 3mM DPC and 150mM NaCl.
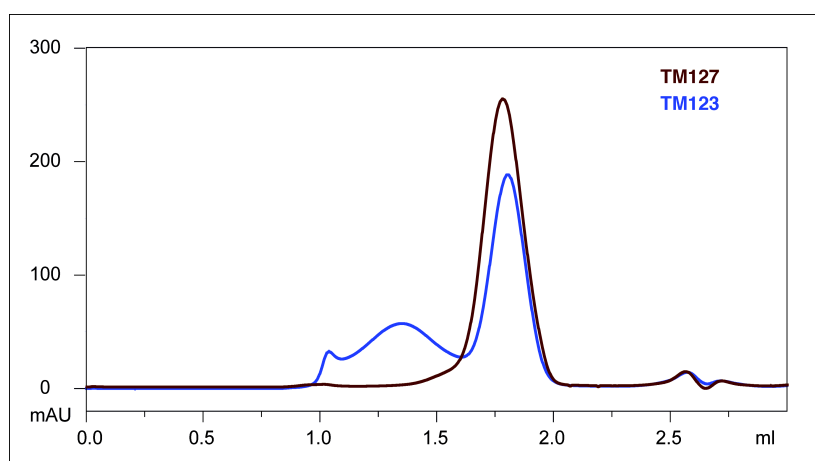

Figure S2: **Overlay of SEC chromatograms from TM123 and TM127.** Freshly prepared TM123 (blue) already forms large soluble aggregates, whereas TM127 (brown) is mostly monomeric. A significant amount of TM123 can already be found in the void volume at around 1.0ml and in the broad peak from 1.1ml to 1.6ml.

Cross-linking experiments to detect the presence of possible oligomers of TM1 or TM2:
The Ste2p fragments TM1, (His)$_6$-TM2 and TM2 were dissolved at 100uM in crosslinking buffer: 40mM KPi pH=7.5, 120mM LPPG, 30mM DPC. Crosslinking reagent bis(succinimidyl)penta(ethylene glycol) (BS(PEG)$_5$) (Thermo Scientific) was dissolved in 40mM KPi pH=7.5 and immediately added at 1mM to the dissolved proteins. The reaction mixture was incubated for 30 minutes at room temperature. Excess cross-linker was quenched with 50mM Tris/HCl pH7.5, and samples were analyzed by MALDI-MS. MS spectra only displayed masses of the free protein as well as the adduct of BS(PEG)$_5$ with a single protein molecule.

NMR Spectroscopy:

The TM1, TM12, TM123 and TM127 constructs all displayed good-quality [^{15}N,^{1}H]-HSQC or TROSY spectra. The corresponding spectra with annotated peaks are displayed below:

[^{15}N,^{1}H]- TROSY Spectra:

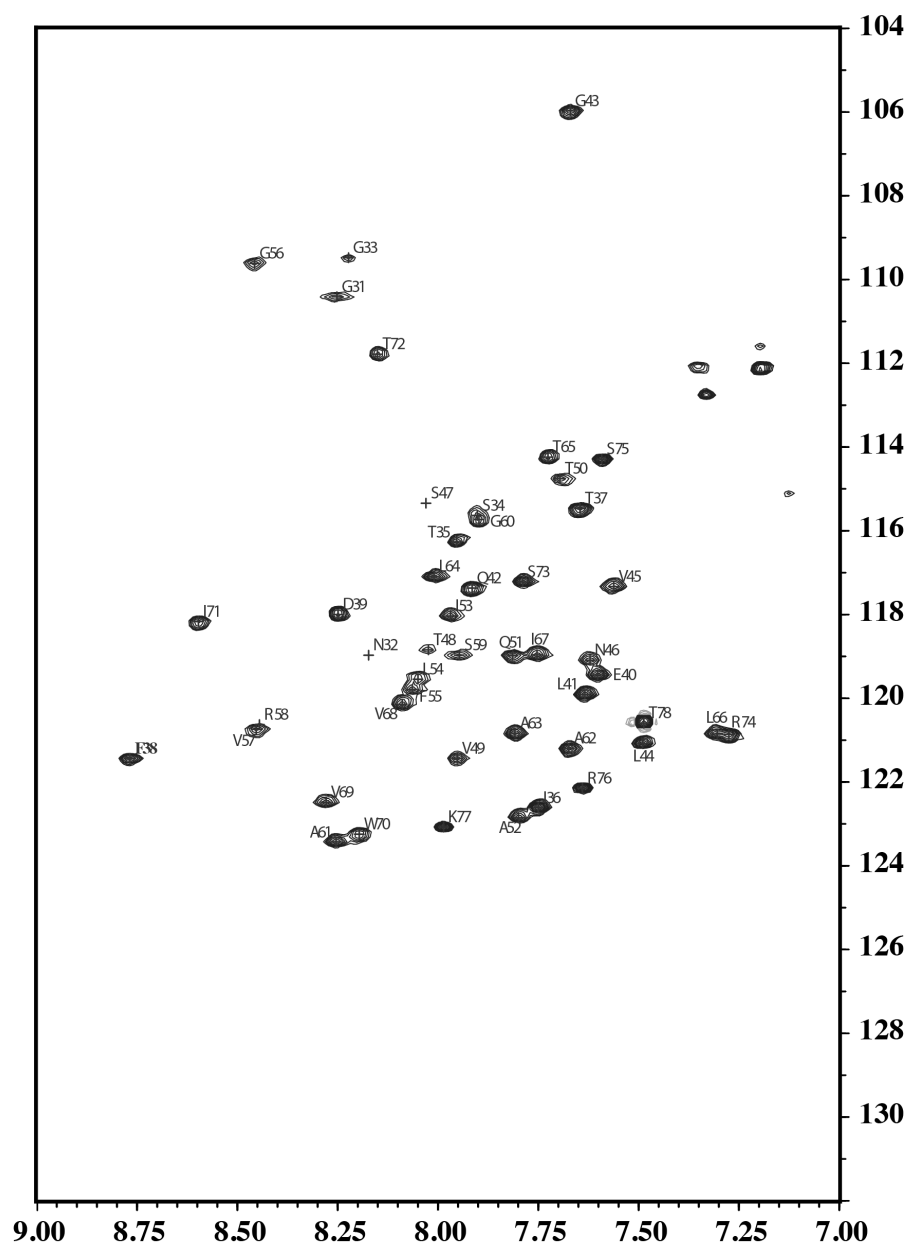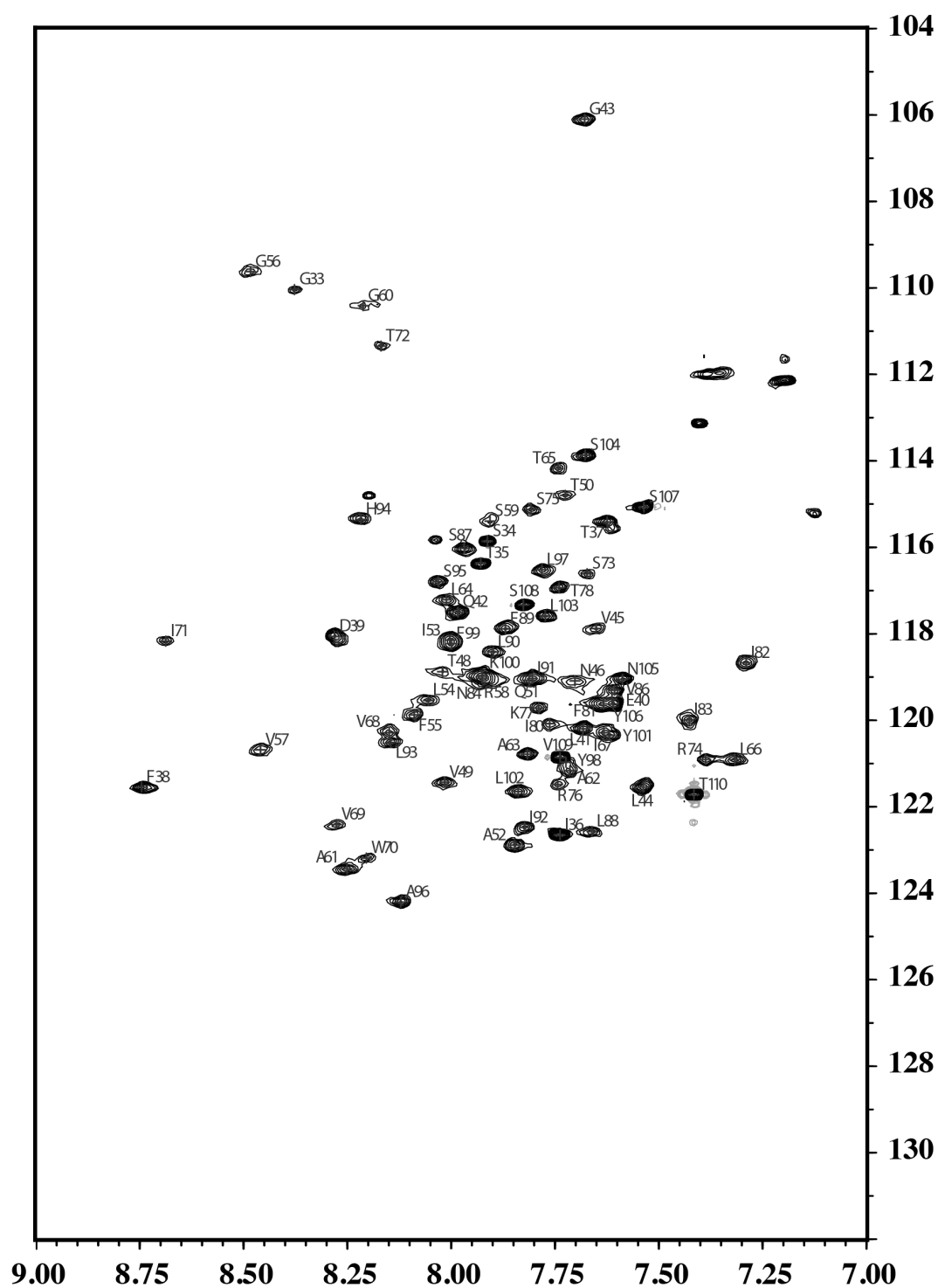Figure S3: **[^{15}N,^{1}H]-TROSY spectrum of TM1 in LPPG/DPC micelles**

Figure S4: [^{15}N,^{1}H]-TROSY spectrum of TM12 in LPPG/DPC micelles

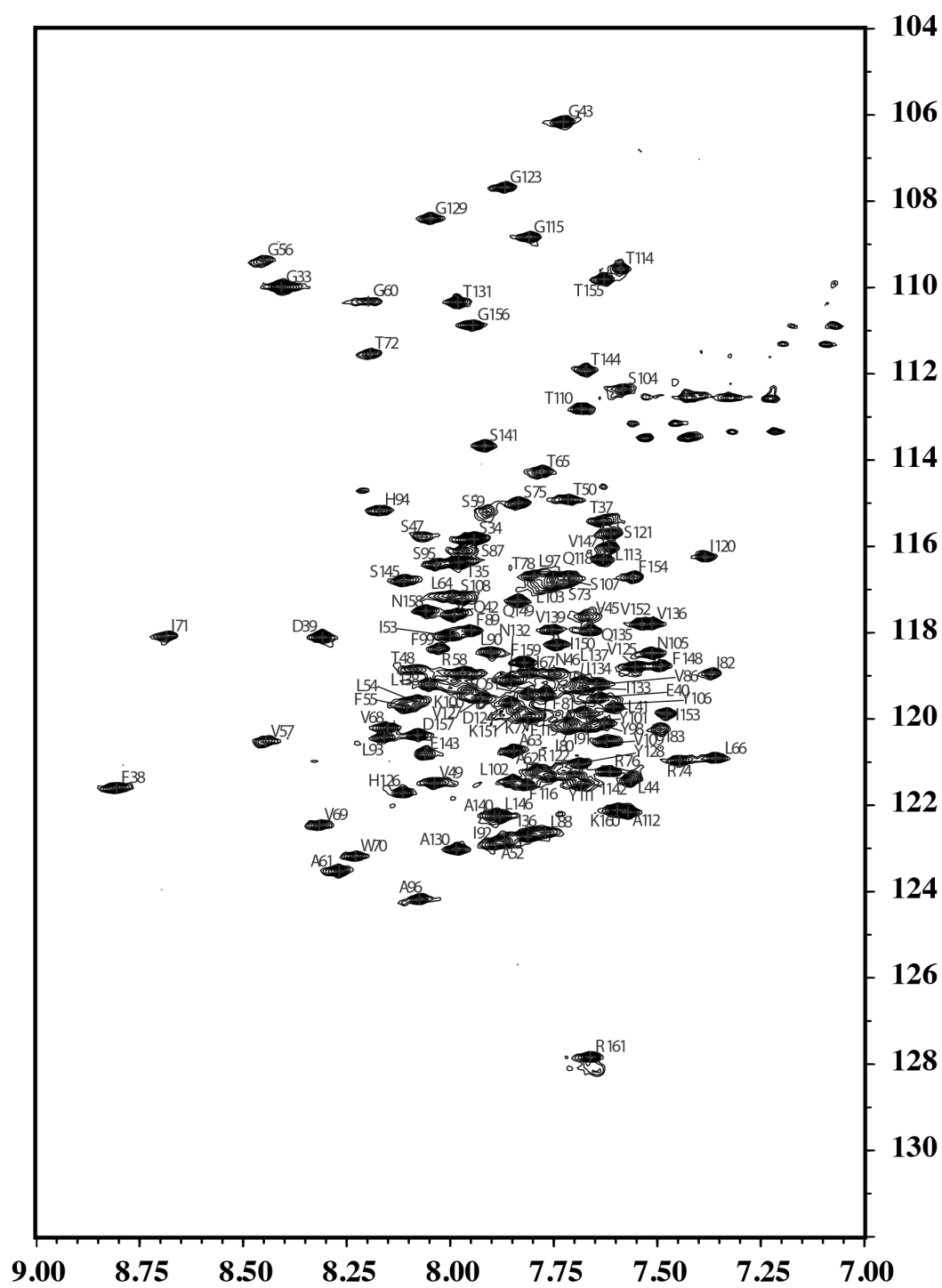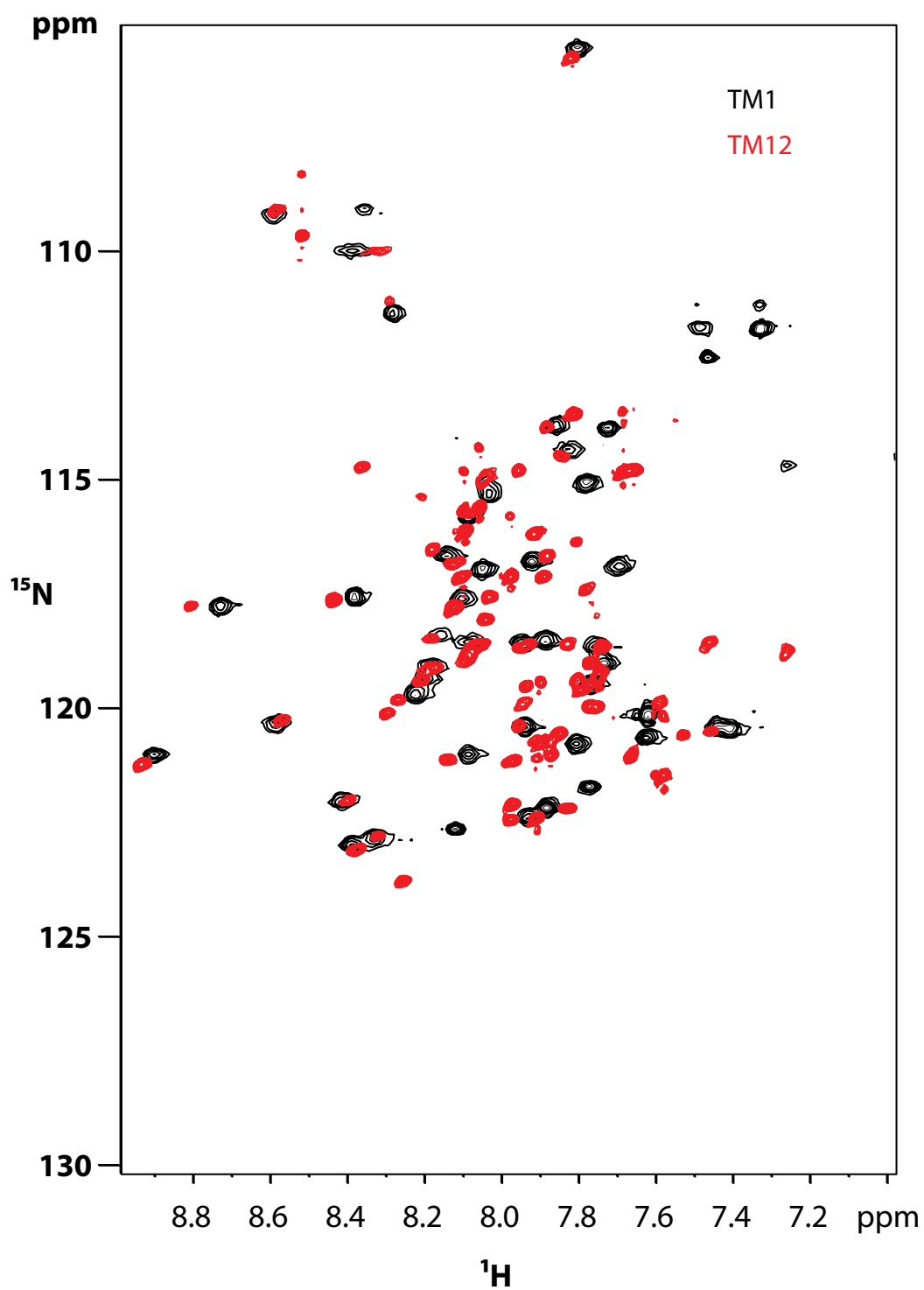Figure S5: [^{15}N,^{1}H]-TROSY spectrum of TM123 in LPPG/DPC micelles

Figure S6: [^{15}N,^{1}H]-TROSY spectrum of TM127 in LPPG/DPC micelles

Figure S7: Overlay of [^{15}N,^{1}H]-TROSY spectra of TM1 (black) and TM12 (red) in LPPG/DPC micelles
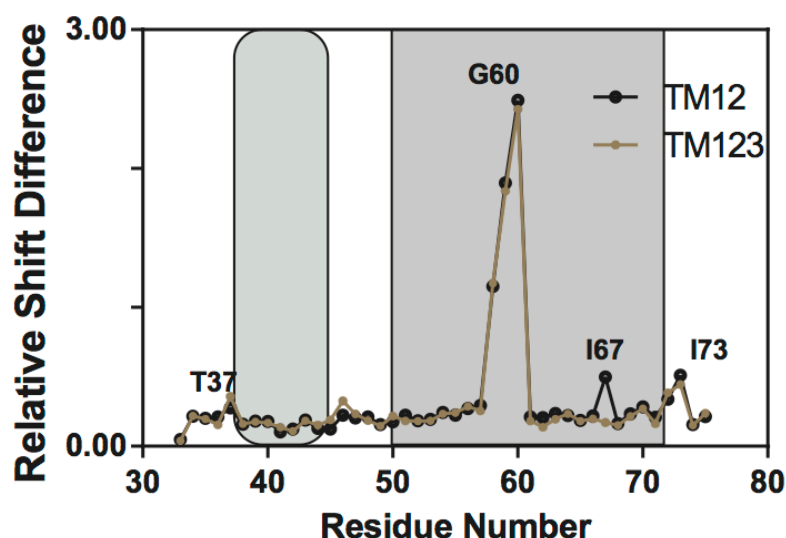
Figure S8: Combined ^{15}N and ^{1}H Chemical shift differences TM1 vs TM12 and TM123

Structural and orientational restraints:

Distances and torsion angles:

Distance restraints were obtained from ^{15}N-resolved NOESY spectra recorded on ^{15}N,^{1}H- and ^{15}N,^{2}H-labeled Ste2p_TM1-TM2 samples with mixing times of 70 and 200 ms, respectively, and from 100 ms ^{13}C-resolved NOESY spectra. In general, ^{15}N- or ^{13}C-resolved NOESY spectra were recorded with non-deuterated and deuterated detergents, respectively. In contrast to the spectra recorded on Ste2p we did not observe significant differences in linewidths in deuterated vs. non-deuterated detergent mixtures. In addition, dihedral angle restraints obtained using the program TALOS+ (30), that uses chemical shifts of ^{1}Hα, ^{13}Cα, ^{13}Cβ, ^{13}C', and ^{15}N nuclei, were added. Peak lists for each spectrum were picked by the program package UNIO'10(6). The automatically picked peaklists were manually edited to remove artifactual peaks (e.g. t_1 noise) or to pick additional weak peaks. The integrated, non-assigned peak list from UNIO'10 was subsequently transferred to CYANA (7), which annotated the peak list in seven iterative cycles using the build-in macro "noeassign". Again, the results from the automatic assignments were carefully checked and edited when necessary.

Peak positions in the ^{13}C- and ^{15}N-resolved NOESY spectra differed for samples recorded in deuterated from those in non-deuterated detergent. To account for that deviation chemical shift positions were related to the corresponding NOESY spectrum both manually and automatically using the sidechain adaptation routine of UNIO'10.

Residual dipolar couplings (RDCs):

RDC samples were obtained by dissolving dinucleotide 2'-deoxyguanylyl-(3',5')-2'-deoxyguanosine (dGpG) in 40mM K_3PO_4 buffer (pH 6.4), 150mM LPPG:DPC (4:1) containing 0.4mM $^{15}N^{13}C^2H$-HIS-N-TM127 and 100mM KCl to ensure G-tetrade formation, to a final concentration of 30mg/ml. Several heating-cooling (45°- 4°C) cycles were necessary to completely dissolve dGpG. Formation of a stable liquid crystal phase was determined by observing the residual ^2H_2O quadrupole coupling on the solvent signal.

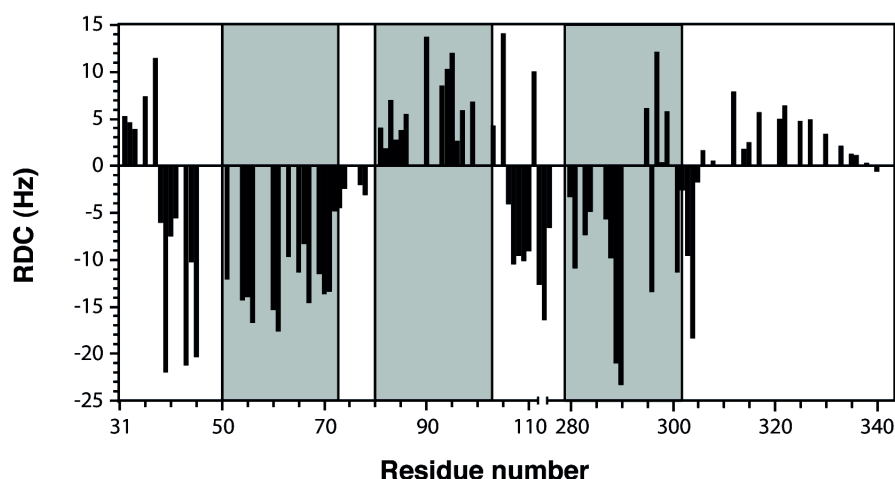Figure S9: **H-N RDCs for TM127**.

NOEs with water and detergent protons:

The topology of TM127 in LPPG/DPC micelles was additionally investigated by measuring NOEs to water protons (water accessibility) and detergent protons (micelle buried segments).
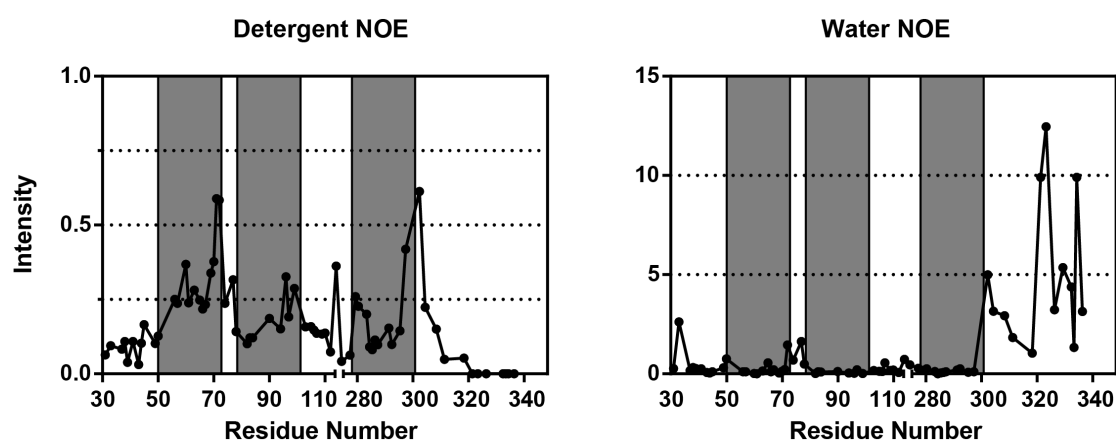

Figure S10: **NOEs to detergent (left) and exchange peaks from water (right) protons for TM127 as detected in the ^{15}N-resolved NOESY spectrum**.

Paramagnetic Relaxation enhancements (PREs):

To obtain long-range distance restraints derived from PREs, *S*-(1-oxyl-2,2,5,5-tetramethyl-2,5-dihydro-1H-pyrrol-3-yl)methyl methanesulfonothioate (MTSL), was attached to unique Cys sites in the protein. Unfortunately, the presence of cysteine residues was incompatible with successive chemical CNBr cleavage, and therefore His-N-TM127, a construct containing the full native N-terminus of the Ste2p receptor, that could be directly expressed (His$_{10}$, S2-T114, T274-L340), was used instead.

Three different single cysteine mutants of the TM127 construct were designed: S47C at the N-terminus of TM1, S75C in the short loop between TM1 and TM2, and S104C at the beginning of the relatively long loop between TM2 and TM7. Signals from residues close in sequence to the spinlabel completely disappeared in two of three cases, indicating quantitative coupling and full functionality of the spin-label for constructs S74C and S104C. For some residues, signal intensities in PRE samples were as large as 120%, suggesting an error of up to 20%.

All PREs were classified in three different classes: Strong PREs, with less than 10% of the original signal intensity (<14Å), medium PREs, with residual peak intensities between 10-80% (14-20Å) and unaffected residues, with residual intensities larger than 80% (>20Å) following methodology originally introduced by the Wagner lab(8).

Structure calculation details and statistics for TM127:

Table S1: NOE distance restraints.

total	728	100.0%
Intraresidue |i-j |= 0	329	45.2%
sequential |i-j| = 1	283	39.0%
short-range |i-j| <= 1	612	84.2%
medium-range 1 < |i-j| < 5	103	14.2%
long-range |i-j| >= 5	13	1.70%

Due to the limited amount of long-range information (see Table S1) the global fold of TM127 could not be calculated based on NOE distance restraints and 166 torsion angle restraints alone. Therefore, a second round of structure calculations was performed using auxiliary sources of structural information available in the form of distance restraints derived from PRE measurements and restraints for residual dipolar couplings.

PRE distances were available in three classes as described above. It was therefore possible to include 26 PRE distances with an upper distance limit of 14.0 Å, 49 distances with an upper limit of 14 Å and a lower limit of 20 Å and 48 PRE distances with a lower limit of 20 Å. PRE distance restraints required cross-checking for compliance with the short- to medium-range NOE restraint network, as well as the restraints for torsion angle restraints.

63 RDC restraints complemented the PRE-derived distance restraints. For the first iteration of structure calculations, artificial upper and lower distance limits were generated to incorporate structural information from soluble paramagnetic spin labels. The restraints were defined between the amide proton of residues with an attenuated signal due to the influence of the spin labels. The approach relied on assumptions made for the detergent micelle environment (detergent LPPG) based on reference literature (Lipfert, 2007) . The micelle was assumed to have an elongated form with a height of 38-40 Å and a length of 56.8-58.8 Å. Upon insertion of TM127 into the micelle in an orthogonal orientation, the center of the micelle was expected at 19-20 Å distance from the solvent-exposed loop regions. In order to represent the micelle nexus, a pseudo residue from the CYANA residue library was utilized. This residue was attached to the amino acid sequence of TM127 via flexible linker of sufficient length. The pseudo residue is insubstantial and cannot cause atom collisions.

Signals strongly influenced by the soluble spin labels and displaying a large degree (>70%) of attenuation received a lower limit of 19 Å to the micelle center. Signals that were not subjected to line broadening resulting from the spin label influence were assumed to be more deeply embedded within the micelle and restrained with upper an upper limit of 15 Å. Signal attenuation was also observed using HNCO experiments. In order to apply information from these measurements to the structure calculation, ambiguous distance restraints were created for atoms H and N of the residue corresponding to an observed attenuated signal, as well as for the carbonyl C of the predecessor amino acid with the aforementioned upper and lower distance limits of 15 Å and 19 Å, respectively. However, the incorporation of distance restraints derived from soluble PREs led to over-restraint structures. The uneven number of observable PREs from soluble spinlabels for different regions in the protein caused the artificially created micelle center to be located outside of the perceived helix bundle. This led to very strong constraints, even at reduced weights, on certain parts of the construct, effectively 'bending' the helices. Restraints from soluble spin labels were therefore omitted from further structure calculations and rather used for qualitative validation for the structures.

In total, the restraints shown in Table S2 were applied in the structure calculation of TM127.

Table S2: **Structure calculations statistics**

Distance restraints		
NOE distance restraints		726
Torsion angle restraints		166
PRE-derived distance restraints	Upper limit only	26
	Upper and lower limit	37
	Lower limit only	47
RDC restraints		63
Structure calculation statistics		
Ave. target function		7.19 Å^2
Ave. backbone RMSD to mean		4.53 Å
Structural clusters		48

In the final structure calculation, 5000 structures were calculated in 10 individual runs with 500 structures each from 10 different random seeds using standard structure calculation routine in CYANA with 20000 torsion angle dynamics steps. The 50 structures with the lowest target function were collected from each run and combined to a bundle containing 500 structures, which was clustered according to the backbone RMSD of helix regions T50-T72, P79-L102 and V276-A299 with a cutoff of 3Å. Clustering resulted in 48 total clusters with the largest containing 95 structures and 11 clusters containing at least 10 structures. 16 clusters with only one structure, 5 clusters with two and 4 clusters with three structures could be observed. The four most prominent clusters with at least 30 structures have been analyzed by back-calculation of the raw PRE and RDC data and subsequently compared to the experimental values, as well as to the back-calculated values for the structure based on a homology model.

Relaxation effects from the water-soluble spin-label:
In addition to the Gd-(DTPA-BMA) studies on TM123 and TM127 we have probed relaxation enhancements for TM1 and TM12. We have measured the effects on (His)$_6$-TM12 and compared it to TM12 in order to investigate whether the addition of the His-tag modifies the interaction with the micelle. Again, all PREs were measured from peak intensities in the HNCO experiment. Presented are relative attenuations for 15mM Gd-(DTPA-BMA) containing samples, taking the corresponding values for the 1 mM Gd-(DTPA-BMA) samples as the reference.
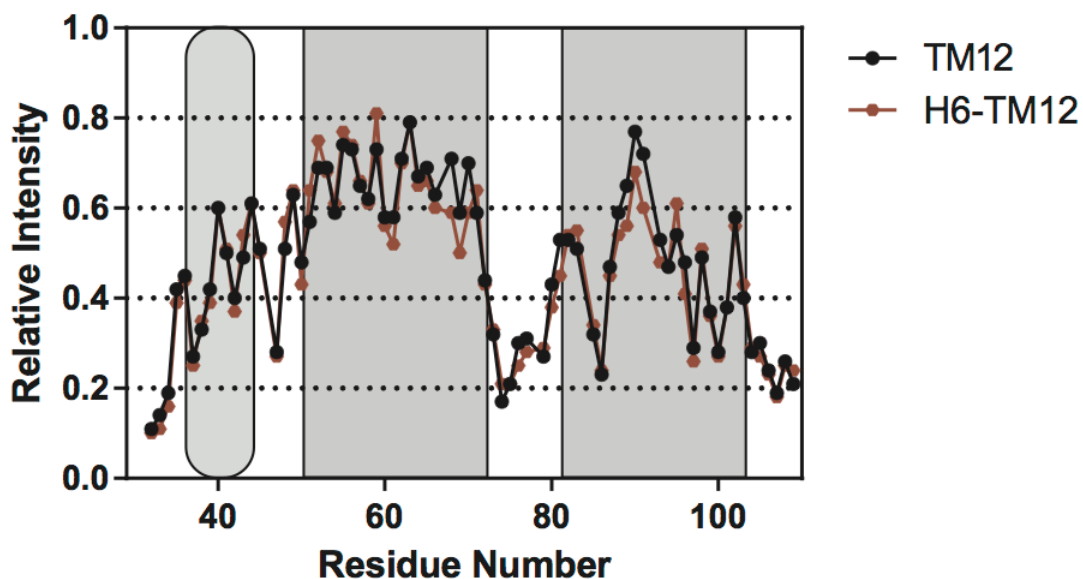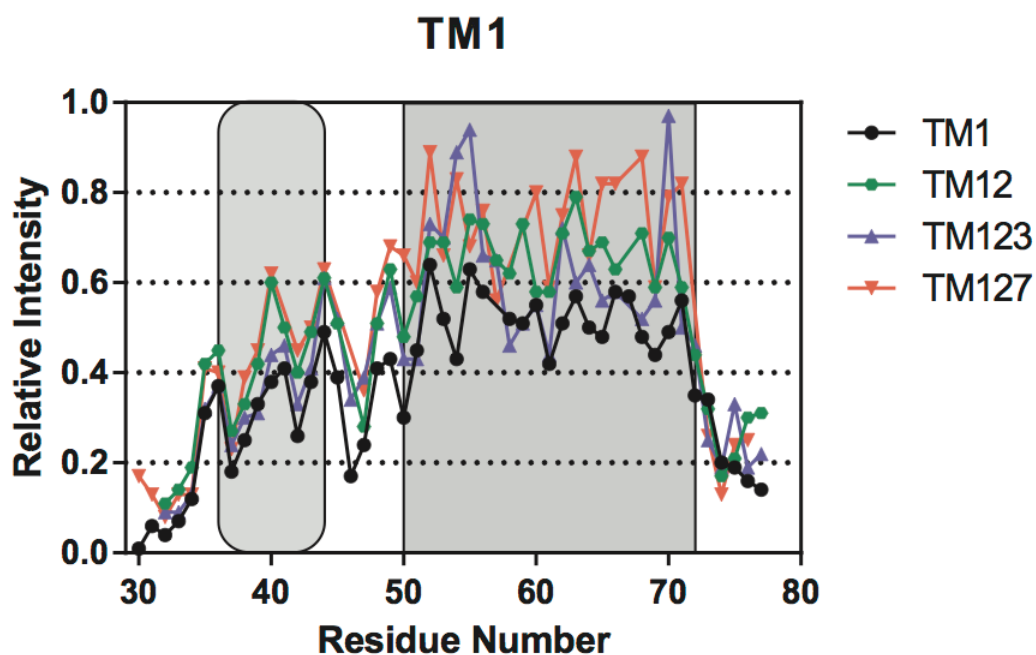
Figure S11: **Water Accessibility**. (A) Relative intensities of TM12 (black) and (His)$_6$-TM12 (red) HNCO peaks after addition of 15mM Gd-(DTPA-BMA). (B) Comparison of attenuations in residues 30-77 caused by 15mM Gd-(DTPA-BMA). The region examined includes the common residues in all investigated peptides: TM1, TM12, TM123 and TM127.

Reconstitution of TM127 into nanodiscs

For reconstitution of TM127 into nanodiscs, lipids, TM127 as well as MSP were mixed in presence of SDS, and the assembly process was triggered through addition of Bio-Beads. The following lipids were used:
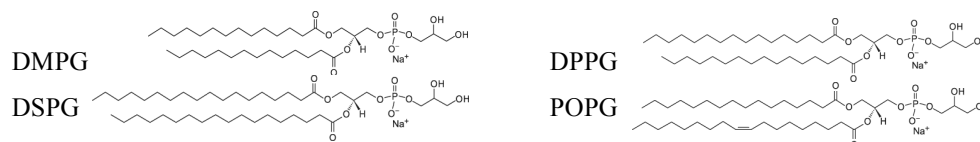

Figure S12: **Chemical structures of lipids used for the nanodiscs.**

In particular, TM127 was expressed as described above and purified by Ni^{2+}-NTA in 2% SDS. Lipids were solubilized at a concentration of 50mM in lipid buffer (20mM Tris/HCl pH=8, 4% SDS, 0.02% NaN3). Cycles of freezing in liquid nitrogen and heating to at least 3°C above the phase-transition temperature of each particular lipid were repeated until a clear solution was obtained. Expression and purification of the membrane scaffold protein MSP1D1ΔH5 was carried out based on the published protocol (4). The MSP/lipid stoichiometry was optimized for each lipid empirically using SEC/MALS. The optimal MSP1D1ΔH5 : lipid ratio was 1:55, 1:30, 1:30 and 1:40 for DMPG, DPPG, DSPG and POPG. Nanodiscs carrying TM127 were assembled based on an established protocol (5). Briefly, TM127, MSP and the particular lipid were mixed in buffer A (20mM Tris/HCl pH=8, 50mM NaCl, 0.02% NaN_3) using a five-fold excess of empty nanodiscs. The concentration of TM127 in the assembly mixture was 5μM and the final concentration of SDS was adjusted to 0.5%. The reconstitution mix was incubated at least 3°C above the lipids phase transition temperature for 30 minutes. To induce the formation of nanodiscs, 0.5g/ml Bio-Beads were added. After the formation of nanodiscs was complete, Bio-Beads were removed by filtration and washed with dilution buffer (20mM Tris/HCl pH=8, 0.02% NaN_3). Therefore the suspension was applied to an empty gravity flow column and the flow through was collected. In order to remove empty nanodiscs, the reaction mix was loaded onto a 1ml HisTrap[TM] HP Ni Sepharose column (GE), equilibrated with buffer A (20mM Tris/HCl pH=8, 50mM NaCl, 0.02% NaN_3). Nanodiscs containing TM127 were purified by gradient elution: 100% buffer B (20mM Tris/HCl pH=8, 50mM NaCl, 250mM Imidazole, 0.02% NaN_3) in 30ml. Fractions containing TM127 nanodiscs were pooled and concentrated using an Amicon Centrifugal Filter (Millipore) with a 10kDa MWCO. Buffer exchange to NMR buffer (50mM KPi pH= 6.4, 0.2mM NaN_3) was performed on a PD-10 Desalting Column (GE Healthcare). NMR samples of TM127/DMPG nanodiscs were concentrated to 300μM using an Amicon Centrifugal Filter (Millipore) with a 10kDa MWCO. NMR samples were characterized by

SEC-MALS on a Superdex 200 Increase 10/300 GL column (GE) with SEC buffer (20mM Tris/HCl pH=7,4, 100mM NaCl, 1mM EDTA 1mM NaN_3) at 0,5ml/min (Fig. S10). The final yield for incorporation of TM127 into DMPG NDs was calculated to be approximately 54% based on the UV absorption of the sample subtracting the UV signal for 2 molecules of the MSP per ND. Nanodisc preparations using lipids different from DMPG were shown by SEC-MALS analysis to not result in intact protein-ND assemblies, and were not further investigated.
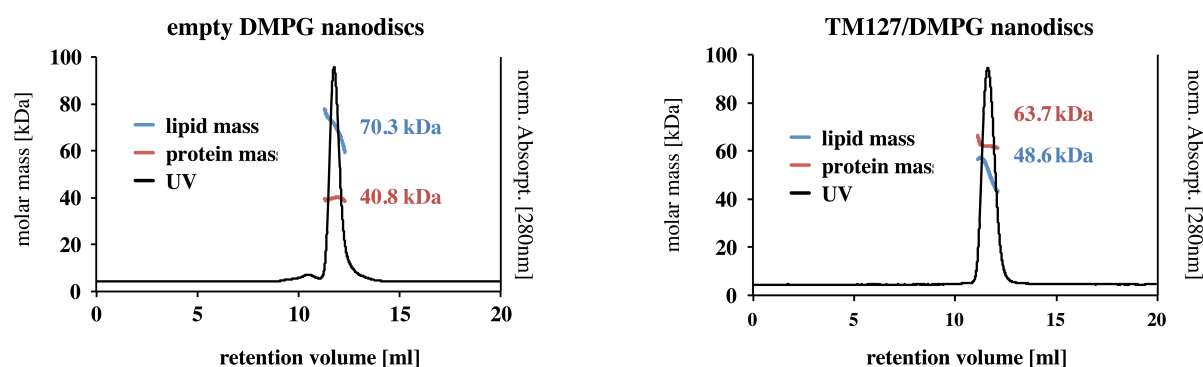

Figure S13: **SEC-MALS analysis of DMPG nanodiscs.** Left: Empty DMPG NDs. Right: TM127/DMPG NDs.

Peaks from TM127 residues in DMPG nanodiscs were broad in the [^{15}N,^{1}H]-TROSY spectra, while peaks from loop or terminal residues were intense and comparably sharp (in contrast to TM127 in LPPG micelles, for which all peaks were clearly visible for the ILV labeled protein:
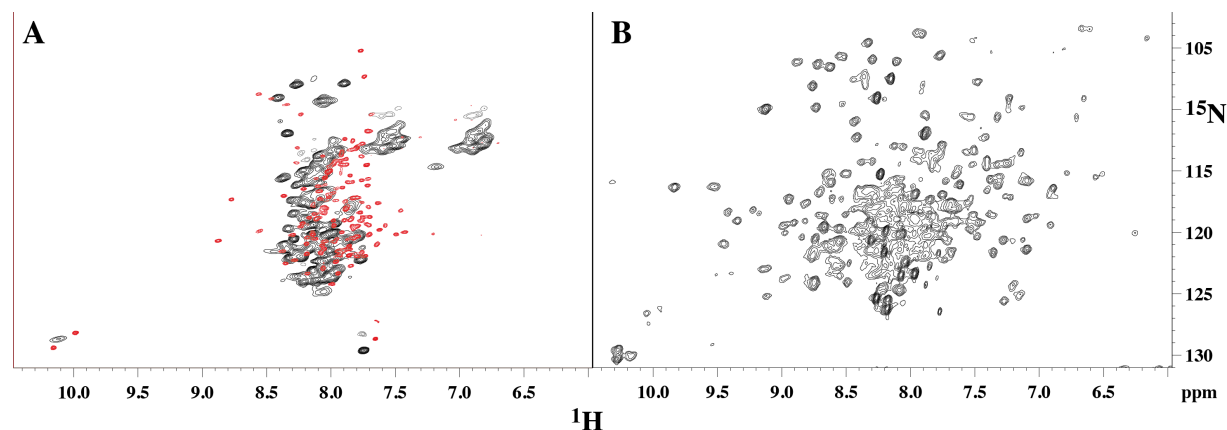

Fig. S14: **[^{15}N,^{1}H]-TROSY spectra of TM127 in DMPG nanodiscs.** A Comparison of TM127 in DMPG nanodiscs (black) and LPPG/DPC micelles (red). B Bacteriorhodopsin in DMPG nanodiscs.

In contrast, [^{13}C,^{1}H]-HSQC spectra revealed spectra of much better quality. Clearly the methyl peaks were again much broader for the protein incorporated into nanodiscs compared to those for the LPPG/DPC micelles. Spectra contained additional peaks that are derived from

the non-deuterated lipids and their degradation products. Otherwise the methyl resonances are observed at locations very similar to those observed for the micelle spectra of TM12 (Fig. S12A) or TM127 (Fig. S12B). Again, a comparison with spectra recorded on bacteriorhodopsin in DMPG nanodiscs (Fig. S12C) displays much better signal dispersion and narrower lines for the 7-TM protein than for TM127 (Fig. S12D).
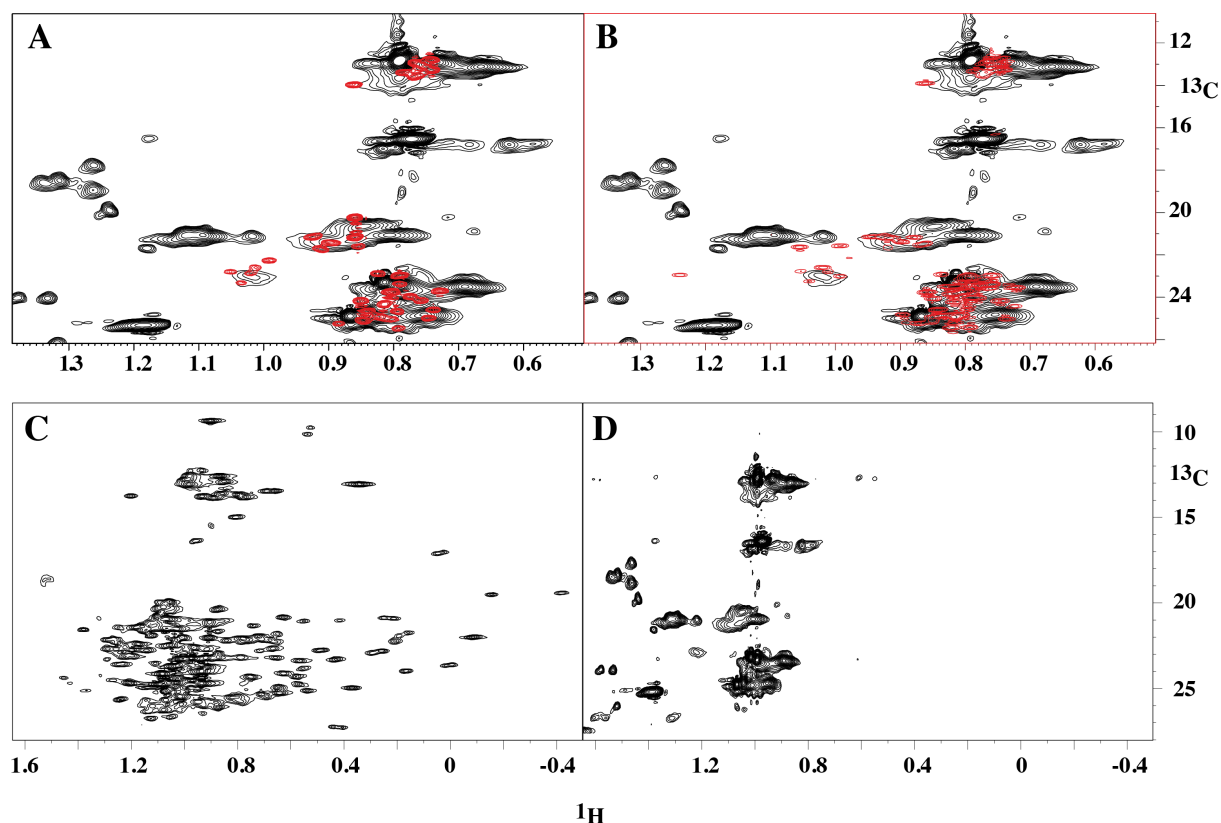

Fig. S15: [^{13}C,^{1}H]-HSQC spectra of TM127 in DSPG nanodiscs. A Comparison of TM127 in DMPG nanodiscs (black) with TM12 in LPPG/DPC micelles (red). B A Comparison of TM127 in DMPG nanodiscs (black) with TM127 in LPPG/DPC micelles (red). C and D [^{13}C,^{1}H]-HSQC spectra of bR and TM127 in DMPG nanodiscs, respectively.

Table S4: Side-chain contributions to predicted ΔG$_{app}$

TM1					TM2			
a.a.	Pos.	Rel. pos.	ΔGaa(i)app		a.a.	Pos.	Rel. pos.	ΔGaa(i)app
A	52	-9	0.02		I	77	-9	-0.11
I	53	-8.1	-0.14		F	78	-8.18	-0.26
L	54	-7.2	-0.38		I	79	-7.36	-0.17
F	55	-6.3	-0.27		I	80	-6.55	-0.21
G	56	-5.4	0.42		N	81	-5.73	0.98
V	57	-4.5	-0.03		Q	82	-4.91	1.02
R	58	-3.6	0.85		V	83	-4.09	-0.05
S	59	-2.7	0.66		S	84	-3.27	0.65
G	60	-1.8	0.47		L	85	-2.45	-0.42
A	61	-0.9	0.12		F	86	-1.64	-0.28
A	62	0	0.13		L	87	-0.82	-0.43
A	63	0.9	0.12		I	88	0	-0.46
L	64	1.8	-0.43		I	89	0.82	-0.45
T	65	2.7	0.42		L	90	1.64	-0.43
L	66	3.6	-0.42		H	91	2.45	1.14
I	67	4.5	-0.32		S	92	3.27	0.65
V	68	5.4	-0.01		A	93	4.09	0.09
V	69	6.3	-0.01		L	94	4.91	-0.4
W	70	7.2	-0.41		Y	95	5.73	-0.06
I	71	8.1	-0.14		F	96	6.55	-0.26
T	72	9	0.04		K	97	7.36	0.57
					Y	98	8.18	-0.18
					L	99	9	-0.35

Σ ΔGaa(i)$_{app}$: **0.72**   Σ ΔGaa(i)app : **0.57**

Hydrophobic moment contribution
ΔG hyd.mom: **0.25**
Length contribution
ΔG length: **-0.63**
ΔG pred$_{app}$ = Σ ΔGaa(i)$_{app}$ + ΔG hyd.mom. + ΔG length = **+0.34**

Positively labeled relative positions (third column) indicate the cytoplasmic side of the membrane whereas negatively labeled positions are indicative of extra-cytoplasmic membrane region. Positive ΔG$_{app}$ values (in kcal/mol) are depicted in red and negative values in green, they are indicative of non-insertion and insertion, respectively. The more preventing values in terms or insertion (> 0.50 kcal/mol) are highlighted in bold (those for R58 and S59).

References:
1.   Geertsma, E. R. and Dutzler, R. (2011) *Biochemistry* **50**, 3272-3278
2.   Hessa, T., Kim, H., Bihlmaier, K., Lundin, C., Boekel, J., Andersson, H., Nilsson, I., White, S. H. and von Heijne, G. (2005) *Nature* **433**, 377-381
3.   Cohen, L. S., Arshava, B., Estephan, R., Englander, J., Kim, H., Hauser, M., Zerbe, O., Ceruso, M., Becker, J. M. and Naider, F. (2008) *Biopolymers* **90**, 117-130
4.   Hagn, F., Etzkorn, M., Raschle, T. and Wagner, G. (2013) *J. Am. Chem. Soc.* **135**, 1919-1925
5.   Gluck, J. M., Wittlich, M., Feuerstein, S., Hoffmann, S., Willbold, D. and Koenig, B. W. (2009) *J. Am. Chem. Soc.* **131**, 12060-12061
6.   Fiorito, F., Herrmann, T., Damberger, F. F. and Wuthrich, K. (2008) *J Biomol NMR* **42**, 23-33
7.   Güntert, P. (2004) *Methods Mol. Biol.* **278**, 353-378
8.   Ross, A., Czisch, M., Cieslar, C. and Holak, T. A. (1993) *J. Biomol. NMR* **3**, 215-224